Astron. Astrophys. 330, 676–684 (1998)

ASTRONOMY
AND
ASTROPHYSICS

Silicon and sulphur chemistry in the inner wind of IRC+10216⋆

Karen Willacy and Isabelle Cherchneff

Department of Physics, UMIST, P.O. Box 88, Manchester M60 1QD, UK

Received 5 June 1997 / Accepted 22 August 1997

Abstract. We present a dynamical and chemical model of the inner wind of the carbon-rich, AGB star IRC+10216. We include the effect of pulsation-driven shocks on the gas envelope close to the stellar photosphere and construct an extended chemical model that includes in particular the chemistry of hydrocarbon species and silicon and sulphur-bearing molecules. The derived theoretical abundances for many molecules are in excellent agreement with values obtained from observations of infrared ro-vibrational molecular lines. We confirm the "parent" character of certain chemical species and show that the inner wind of IRC+10216, and more generally of evolved AGB stars, is an active dynamical and chemical region where molecules are formed and processed.

Key words: molecular processes – stars: AGB – stars: individual: IRC+10216

1. Introduction

Towards the end of their time on the Asymptotic Giant Branch (AGB), stars develop a strong stellar wind due to a combination of stellar pulsations and dust grain condensation. These winds result in extended circumstellar envelopes which are extremely rich in molecules. Indeed, more than 40 chemical species have been so far observed at infrared (IR) and millimetre (mm) wavelengths in the envelope of the well-studied, carbon-rich, AGB star IRC+10216 (Olofsson 1997). The chemical processes responsible for this molecular wealth are dependent on the position in the envelope. In the stellar photosphere and at the inner boundary of the envelope, the high gas density and temperature ensure thermal equilibrium (TE) and the molecular content of the gas can be assessed easily when its elemental chemical composition, temperature and total pressure are specified. TE is suppressed very close to the photosphere because of the action of pulsation-driven shocks propagating outwards. Furthermore the regions of strong shock activity correspond to the locus of grain formation and wind acceleration. We refer to this region as the inner envelope (or inner wind) which extends over a few stellar radii. At larger radii ($\sim$ 10 to 100 $R_\star$) the newly formed dust grains interact with the cooler gas of the steady, fully-accelerated wind. Depletion of certain molecular/atomic species may result from such an interaction and these layers are referred to as the intermediate envelope. At still larger radii ($> 100\,R_\star$), the gas parameters resemble those of the interstellar medium and the penetration of ultraviolet interstellar photons and cosmic rays induce a chemistry governed by photochemical processes. This region is often referred to as the outer envelope of an AGB star.

Most of the studies of the chemistry of AGB circumstellar envelopes have focused on IRC+10216 outer envelope and several photochemical models have been developed (Cherchneff et al. 1993, Cherchneff & Glassgold 1993, Millar & Herbst 1994) with the purpose of reproducing molecular abundances derived from mm observations. Usually the abundances of the dominant species entering the outer layers are set by using abundances derived from IR observations which probe the deeper layers of the wind. These values normally agree with the scenario that the most dominant species CO, N_2, HCN and C_2H_2 travel through the inner and intermediate envelopes relatively unaffected. Their abundances entering the outer envelope are therefore very close to their TE photospheric values.

This is not the case for a few species observed to be present close to the star at IR wavelengths but for which the observed abundances are quite different from their TE values in the photosphere. For example, SiO IR ro-vibrational lines have been observed by Keady & Ridgway (1993) and its observational abundance is a few ten times larger than the TE values we calculated for parameters characteristics of the IRC+10216 stellar photosphere. For CS, Boyle et al. (1994) derive an observational value three times smaller than our calculated TE abundance. In the case of SiC_2, Gensheimer et al. (1995) predict an inner envelope abundance at least ten times smaller than the photospheric TE value from full synthesis mm maps. These discrepancies suggest that there must be some important processes taking place in the inner envelope that affect certain chemical species before their entry into the intermediate and outer envelopes of the star.

In this paper we model the inner envelope of IRC+10216 using semi-analytical methods derived by Bertschinger & Cheva-

Send offprint requests to: I. Cherchneff

⋆ Table 5 is only available in electronic form at the CDS via anonymous ftp to cdsarc.u-strasbg.fr (130.79.128.5) or via http://cdsweb.u-strasbg.fr/Abstract.html

Table 1. The stellar parameters assumed for IRC+10216. The parameters γ and α are defined as in Cherchneff et al. (1992)

$T_\star$	2300 K	$L_\star$	2.5×10^4 $L_\odot$
$R_\star$	7.0×10^{13} cm	$M_\star$	2 $M_\odot$
P	650 days	n(r_s)	3.7×10^{14} cm^{-3}
r_s	$1.2\times$ $R_\star$	α	0.6
$\gamma = \Delta v/v_e$	0.89		

lier (1985) and Cherchneff et al. (1992). We consider the effect of pulsation-driven, periodic shocks on the dynamics of the inner envelope and the gas chemistry. Starting from the photosphere, we follow the chemistry out to $\sim$ 5 $R_\star$, concentrating in particular on silicon- and sulphur-bearing molecules. In the next section we describe our model for the gas dynamics and discuss the reactions which have been included in the chemical scheme. Results are presented in Sect. 3 and compared to observational data. In Sect. 4 we briefly discuss the impact of dust grain formation on our model.

2. The model

2.1. Dynamics

Evolved, low-mass stars experience periodic pulsations which cause large amplitude compressional waves to propagate outward and to steepen into shocks outside the stellar photosphere (Hinkle et al. 1982, Willson & Bowen 1984, Bowen 1988). These periodic shocks travel through the inner layers of the envelope and alter dramatically both the temperature and the density of the gas (Cherchneff & Tielens 1994). Because the preshock gas is molecular and relatively cool ($\sim$ 2000 K), the energy deposited by the shocks into the gas is lost mainly via the dissociation of molecular hydrogen, H_2, and adiabatic expansion (Fox & Wood 1985). Layers of gas are then accelerated upwards (the hydrodynamical postshock zone) but decelerate and eventually almost fall back to their initial position under the influence of stellar gravity, leading to the formation of a quasi-stationary layer close to the stellar photosphere. The cycle is then repeated with the next pulsation and the gas parcels gradually move outwards and eventually escape from the shocked regions.

The dynamics of the shocked regions is modelled in two stages. We assume that a shock forms at the shock formation radius, r_s, outside the stellar photosphere and that its strength, Δv, is damped as the shock travels outwards (Cherchneff et al. 1992, Cherchneff & Tielens 1994). We study the effect of the shock on the gas considering the postshock region and its various cooling processes, and we adopt a Lagrangian formalism to describe the hydrodynamical cooling zone.

First we derive the variation of the gas parameters (temperature, density and velocity) in the "chemical" cooling layer of the postshock region. Starting with the preshock gas parameters, we assume the Rankine-Hugoniot jump conditions applied to a diatomic gas to derive the parameters of the cooling region just after the shock front. We then assume thermal cooling by H_2 dissociation via collision with H atoms until the parameters have reached the values where hydrodynamical cooling starts. The length of the "chemical" cooling layer is defined by the collisional dissociation of H_2 and the dominant dissociative reaction for molecular hydrogen is

$$H + H_2 \rightarrow 3\,H \qquad (1)$$

The rate for Reaction (1) is

$$k_1 = 3.78\,10^{-8} \left(\frac{T}{300}\right)^{-0.5} exp(-53280/T) \quad \mathrm{cm^3\ s^{-1}} \qquad (2)$$

where T is the gas kinetic temperature (see Table 5). The H_2 dissociation length is defined as

$$l_D = \frac{1}{k_1\, n(H)} \times \frac{V_{shock}}{N_{jump}} \qquad (3)$$

where $n(H)$ is the atomic hydrogen number density, V_{shock} is the shock velocity in the stellar rest frame and N_{jump} is the density jump in the shock front given by the Rankine-Hugoniot jump conditions.

Second we model the hydrodynamical postshock region and its quasi-ballistic trajectory following a formalism derived by Bertschinger & Chevalier (1985) who solve for the continuity, momentum and energy equations of a periodically shocked, adiabatically expanding gas subjected to the stellar gravitational field. We calculate the parameters (temperature, T, number density, n, and velocity, v) as a function of phase p (with $p = t/P$ where t is the time and P the stellar pulsation period) for Lagrangian parcels of gas. Strictly periodic motion of the gas (i.e., no mass loss) is assumed and this condition holds to a first approximation in the stationary region close to the photosphere.

Table 1 lists the stellar parameters used in the model for IRC+10216. The α exponent describing the gas temperature dependence and the γ coefficient relating the shock strength to the local escape velocity are the same as in the "standard model" defined by Cherchneff et al. (1992). Our choice of shock formation radius r_s is arbitrary but in accord with values used by Bowen (1988). Table 2 gives the preshock, jump, and postshock gas parameters for the various shock strengths considered in this study. The corresponding Mach numbers ($M = \Delta v/a$ where a is the gas thermal sound velocity) and the dissociation length, l_D, are also listed. The shock strengths represent a 20 kms^{-1} shock at r_s whose amplitude is damped as it travels outwards.

The variation of T and n with phase, p, for the gas excursion induced by a 20 kms^{-1} shock is shown in Fig. 1. The adiabatic expansion is very efficient at cooling the gas (even below the gas radiative equilibrium temperature at large p values, as first mentioned by Bowen (1988)). Fig. 2 represents the excursions of various gas layers located at different positions in the envelope which correspond to the damped shock strengths listed in Table 2.

The model (consisting of the immediate postshock region and excursion for one shock strength at one position in the envelope) is run over two pulsation cycles to check that periodicity

Table 2. Preshock, shock front and excursion gas temperature and number density for the various shock strengths Δv (or Mach number M) chosen in the model. l_D is the H_2 dissociation length given by Equation (3).

Δv	Radius	M	Preshock		Shock Front		Start of excursion		Dissociation Length
(kms^{-1})	($R_\star$)		T_0 (K)	n_0 (cm^{-3})	T (K)	n (cm^{-3})	T (K)	n (cm^{-3})	l_D (cm)
20.0	1.2	6.7	2062	3.68 (14)	19722	1.98 (15)	4530	6.25 (15)	1.6
15.9	1.9	6.1	1565	2.25 (13)	12646	1.19 (14)	3303	3.37 (14)	1.6 (4)
14.8	2.2	5.9	1433	1.03 (13)	11048	5.40 (13)	2989	1.51 (14)	4.8 (6)
13.3	2.7	5.7	1267	3.67 (12)	9086	1.91 (13)	2611	5.19 (13)	2.0 (8)
12.6	3.0	5.5	1190	2.24 (12)	8218	1.16 (13)	2440	3.11 (13)	3.2 (6)
11.7	3.5	5.4	1085	1.12 (12)	7100	5.73 (12)	2198	1.51 (13)	2.7 (5)
9.8	5.0	5.0	876	2.66 (11)	5079	1.33 (12)	1544	2.13 (12)	7.4 (6)

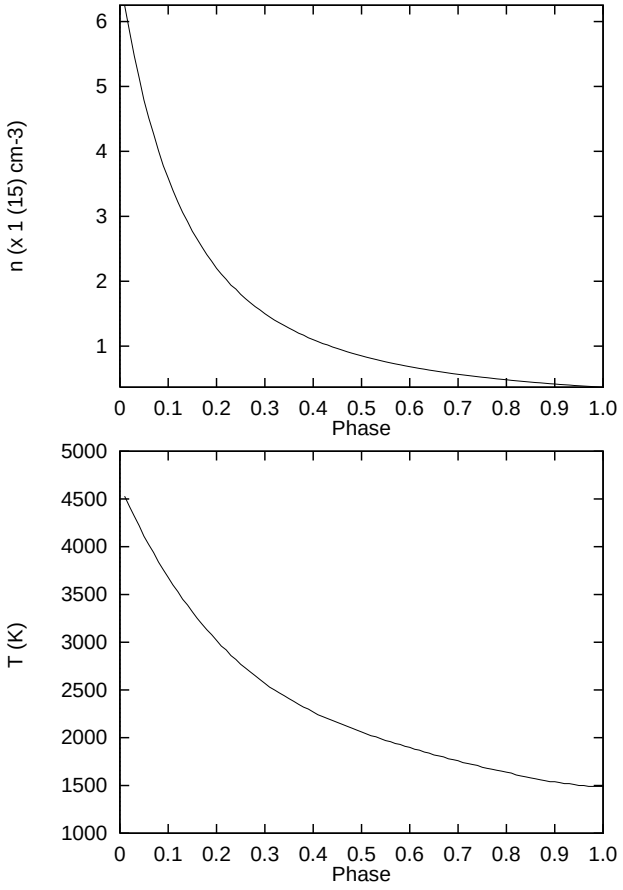

Fig. 1. The variation of the gas temperature T and number density n as a function of phase p for the excursion induced by a 20kms^{-1} shock.

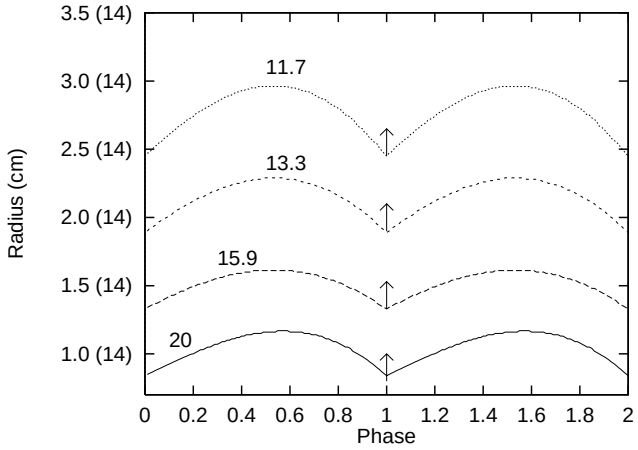

Fig. 2. Gas excursions induced by different shock strengths (in kms^{-1}). The arrows show where the gas is shocked.

is obeyed. The output abundances for one model are used as the input to that for the next slowest shock strength and are rescaled according to the new local gas number density. More details on the dynamical model are given in Cherchneff & Tielens (1997).

2.2. Chemistry

The chemistry of 53 species involving the elements H, C, S, O, N, and Si is followed in the immediate postshock regions and excursions. The chemistry and hydrodynamics of the wind have been decoupled because chemical species, apart from H_2, do not participate much in cooling the postshock gas. Furthermore, radiation pressure on molecules is inefficient at accelerating the gas (Cherchneff et al. 1991) and therefore the wind dynamics are not significantly altered by the gas molecular component. A complete treatment of the postshock regions (chemistry, radiative transfer and hydrodynamics) would be more accurate but quite complex to implement and we feel that our analytical description of the flow hydrodynamics is sufficient to reproduce the changes in wind parameters and to concentrate on the wind chemistry. The elemental composition of IRC+10216 is assumed to be solar except for carbon and we assume a C/O ratio of 1.5. All the chemical compounds considered and their initial TE concentrations at r_s are listed in Table 3. The full chemical scheme is listed in Table 5 and consists of 564 reactions. The various chemical processes considered are termolecular and bimolecular neutral-neutral reactions. No photo-processes (dissociation or ionisation) are considered due to the very weak ultraviolet stellar radiation field and the inferred absence of a chromosphere for IRC+10216. Most of the rates used are taken from the UMIST database RATE95 (Millar et al. 1997). Other rates are from Baulch et al. (1992), Cherchneff et al. (1992), Mick et al. (1994) and from the NIST database (Mallard et al.

Table 3. TE chemical concentrations at r_s [a (b) represents a $\times$ 10^b].

Species	n (cm^{-3})	Species	n (cm^{-3})
H_2	2.44 (14)	CH_4	2.55 (6)
H	6.88 (13)	N	5.85 (5)
He	5.53 (13)	SiN	2.70 (5)
CO	3.48 (11)	SiC	1.80 (5)
C_2H_2	5.74 (10)	HCS	1.69 (5)
N_2	2.31 (10)	HCSi	8.05 (4)
C_2H	2.01 (10)	HNSi	6.15 (4)
HCN	1.88 (10)	SiH_2	3.93 (4)
Si	1.35 (10)	$SiCH_2$	3.43 (4)
CS	4.68 (9)	C_3H_2	2.98 (4)
SiS	3.68 (9)	NH	7.58 (3)
C_3H	2.75 (9)	H_2O	6.80 (3)
S	3.18 (8)	NH_3	3.32 (3)
CN	1.93 (8)	NH_2	2.77 (3)
SiC_2	1.74 (8)	HCO	2.40 (3)
C	1.52 (8)	SiH_3	1.69 (3)
SiH	7.20 (7)	S_2	1.41 (3)
HS	4.96 (7)	NS	2.55 (2)
C_3	4.38 (7)	OH	1.96 (2)
C_2	4.19 (7)	O	3.93 (1)
CH_3	1.76 (7)	H_2CO	1.80 (1)
C_4H_2	8.90 (6)	CO_2	1.99 (0)
C_4H	8.90 (6)	NO	7.36 (-2)
CH_2	8.12 (6)	SiH_4	4.96 (-2)
CH	6.95 (6)	SO	4.60 (-2)
SiO	6.84 (6)	O_2	4.24 (-10)
H_2S	2.65 (6)		

1994). Because of the large gas densities in the inner envelope, each reaction is assumed to proceed in both the forward and reverse directions. Where no reverse process is documented the reverse reaction rate, k_r, is calculated from the thermodynamics of the reaction and is given by

$$k_r = AT^n C^{\Delta\nu} exp\left\{\frac{\Delta G_R - E_\alpha}{RT}\right\} \quad (4)$$

(Cherchneff et al. 1992) where A, n and E_α are the Arrhenius parameters for the forward reaction, $C = N \times 10^6/RT$ is the conversion factor from atmosphere to cm^{-3} units, ν the stochiometric factor, N is the Avogadro number, R the perfect gas constant, and T the gas temperature. ΔG_R is the Gibbs free energy for the forward reaction at 1 atmosphere of total gas pressure and is calculated from the Gibbs free energies of formation, ΔG_f, of the reactants and products. These data were taken from the JANAF thermochemical data tables (Chase et al. 1985) and extrapolated to large temperatures assuming a constant heat capacity, C_p, for $T > 6000$ K. Thermochemical data for HCSi are taken from Allendorf & Mellius (1992). Where no published data is available the Gibbs free energies are estimated using the group additivity method of Benson (1976). For a long time SiC_2 was considered to have a linear structure and thermochemical data are tabulated in the JANAF tables for linear SiC_2. To account for the newly discovered, more stable cyclic structure of SiC_2, we have assumed the same heat capacities as for linear SiC_2 but have corrected the enthalpy of formation by an amount -3.16 kcal mol^{-1} (Fitzgerald et al. 1986) and included the effect of the changed symmetry in the entropy.

Among the reactions involving silicon- and sulphur-bearing species, only a few have documented reaction rates. To overcome the difficulty of the lack of experimental or theoretical data we have considered processes which energetics predict to be exothermic and have estimated their rates from similar reactions involving covalent species i.e. oxygen for sulphur and carbon for silicon (see Table 5). We have not rescaled the rates according to the change in the reduced mass of the system because the variations in the rates were all less than a factor 2 and had negligible effect on the Si-S chemistry.

Some of the rates for the gas collider reactions have been measured at temperatures similar to those encountered in the inner wind and were obtained from the NIST database. Where the rates are not available we have made the "educated" guess of

$$k_{collider} = 10^{-10} exp(-48000/T) \ \ \mathrm{cm^3 s^{-1}} \quad (5)$$

which is typical of many gas collider processes.

3. Results

The results for a variety of species are presented in Table 4. Also listed in the table are abundances derived from IR and mm observations of IRC+10216. We consider that both theoretical and observational abundances agree very well when they differ by at most a factor of seven. This can be understood by the uncertainty introduced in our model by an oversimplified flow dynamics and estimated chemical reaction rates. Furthermore, observational values are derived assuming certain models for the wind that may not represent with great accuracy the actual inner envelope.

Our results for the "parent" molecules CO and C_2H_2 are in excellent agreement with the IR observational of Keady et al. (1988) and Keady & Ridgway (1993), and confirm the fact that these two molecules travel through the inner envelope keeping their TE photospheric abundances. This is not the case for CS and we discuss below the non-equilibrium chemistry of this species. A discrepancy exists for HCN for which our theoretical abundance is about an order of magnitude smaller than that derived by Wiedemann et al. (1991). We ascribe this difference to the uncertainty in the estimated rates of a few chemical processes in which HCN is involved and to the intrinsic uncertainties in abundance determination from observations. We discuss below the results for some chemical families.

3.1. Atomic and molecular hydrogen

Molecular hydrogen is expected to be the dominant molecular species in cool circumstellar environments. However, its detection is prevented because of the lack of a permanent dipole moment. Zuckerman et al. (1980) have searched for the 21 cm line of atomic hydrogen in the envelope of IRC+10216 and they

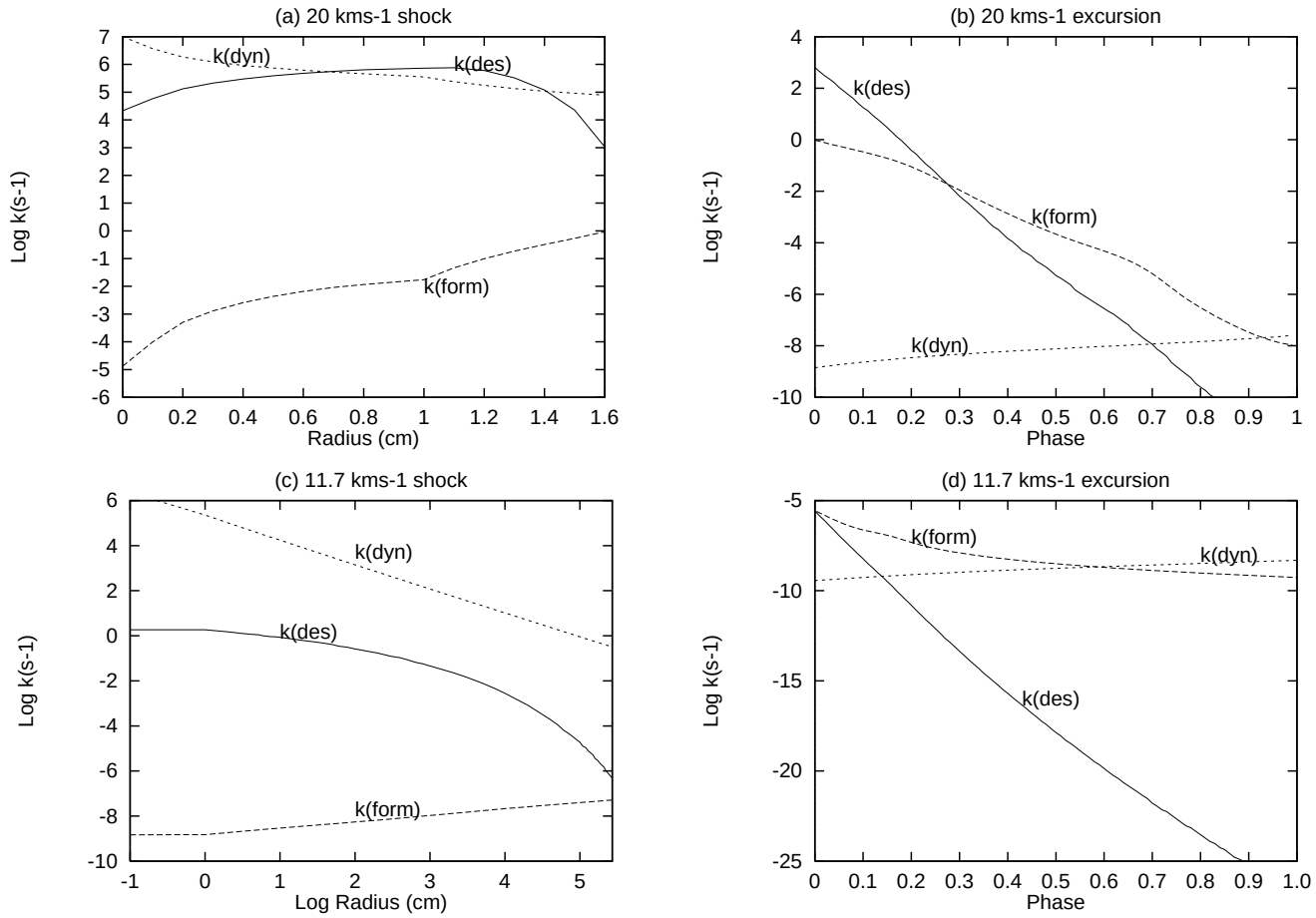

Fig. 3a–d. Net chemical rates for H_2 formation ($k(form)$) and destruction ($k(des)$) and the inverse of the dynamical timescale $k(dyn)$ for the postshock region and excursion induced by two shock velocities, 20 kms^{-1} (**a** and **b**) and 11.7 kms^{-1} (**c** and **d**).

derived an upper limit of only a few percent of the total envelope mass, indicating that hydrogen is likely to be in molecular form in the outer envelope of the star. The electric quadrupole transitions of H_2 have been searched for by Keady & Ridgway (1993) but were not detected.

As seen in Table 4, TE calculations imply that H_2 is more abundant than H at r_s but the H_2-to-H ratio changes dramatically in the inner shocked region. Fig. 3a–d represents the net chemical reaction rates for H_2 destruction, $k(des)$, and H_2 formation, $k(form)$, given by Reaction (1) and its reverse process for the immediate postshock region and the excursion associated with two shock strengths, 20 and 11.7 kms^{-1}. Also plotted is the inverse of the flow dynamical time scale, $k(dyn)$, defined as $k(dyn) = v/r$ where v is the local flow velocity and r is the position in the flow. In the fast shock, $k(dyn)$ is large and the H-H_2 chemistry cannot proceed in the immediate postshock region, except for some H_2 destruction by Reaction (1) (see Fig. 3a–d-a). At the very beginning of the hydrodynamical cooling region (Fig. 3a–d-b), $k(dyn)$ becomes small (phase p = 0.01 corresponds to a flow time of 5.6×10^6 s) and the chemistry acts quickly to destroy H_2 effectively. At longer phase, the gas temperature and number density decrease and chemistry is less efficient but still reforms H_2 until freeze-out occurs at $\sim p$ = 0.9, i.e. $k(dyn)$ is again larger than $k(des)$ and $k(form)$ and the H_2 concentration now follows the gas density variation. For slower shock speeds (see Fig. 3a–d-c and 3a–d-d), the flow dynamics dominate the chemistry in the immediate postshock region and the species number densities remain unchanged after the passage of the shock front. In the hydrodynamical postshock region, H_2 reforms but less efficiently due to the smaller gas temperature and number density and freeze-out occurs at a smaller phase. For very slow shocks, the flow dynamics governs the entire postshock region and chemistry is inactive.

This analysis applies to other molecules and a schematic representation of the various chemical regions in the oscillation described above is presented in Fig. 4 for the gas excursion induced by a 20 kms^{-1} shock. For slower shock velocities, the freeze-out zone will gradually take over the "fast chemistry" region.

Two important conclusions can be drawn. Firstly, the abundances calculated for each radius in the inner wind are governed by the chemistry occuring in the excursion ($\equiv$ the hydrodynamical cooling part of the postshock region) and *not* in the immediate postshock region. This is due to the existence of the

Table 4. Calculated fractional abundances (relative to the total gas number density) for a variety of species versus shock strength (and position in the envelope). Input abundances at r_s are those of Table 1. Observational abundances are taken from (1) Keady & Ridgway (1993), (2) Gensheimer et al. (1995), (3) Boyle et al. (1994), (4) Keady et al. (1988), and (5) Wiedemann et al. (1991)

Species	TE ($r < 1.2$ R$_\star$)	20 kms^{-1} (1.2 R$_\star$)	15.9 kms^{-1} (1.9 R$_\star$)	13.3 kms^{-1} (2.7 R$_\star$)	11.7 kms^{-1} (3.5 R$_\star$)	9.8 kms^{-1} 5.0 $R_\star$	Observations
H	1.87 (-1)	1.68 (-3)	2.18 (-5)	6.03 (-3)	7.83 (-2)	1.55 (-1)	
H_2	6.61 (-1)	8.32 (-1)	8.33 (-1)	8.28 (-1)	7.61 (-1)	6.90 (-1)	
He	1.51 (-1)	1.67 (-1)	1.67 (-1)	1.66 (-1)	1.60 (-1)	1.54 (-1)	
Si	3.68 (-5)	1.95 (-5)	2.18 (-5)	2.59 (-5)	2.56 (-5)	2.45 (-5)	
S	8.65 (-7)	8.55 (-13)	1.19 (-18)	3.79 (-16)	8.36 (-16)	2.47 (-18)	
C	4.11 (-7)	1.56 (-13)	9.94 (-19)	4.58 (-17)	5.87 (-17)	3.65 (-17)	
SiC	4.90 (-10)	1.12 (-11)	5.28 (-15)	6.18 (-21)	8.61 (-24)	1.41 (-28)	
SiC_2	4.72 (-7)	9.18 (-9)	8.44 (-9)	5.88 (-9)	3.25 (-9)	1.36 (-9)	< 5.0 (-8)[2]
CS	1.27 (-5)	1.13 (-12)	5.19 (-14)	1.89 (-7)	7.09 (-7)	5.96 (-7)	4.0 (-6)[1]
SiS	1.00 (-5)	2.62 (-5)	2.62 (-5)	2.59 (-5)	2.45 (-5)	2.37 (-5)	4.0 (-5) - 4.0 (-6)[3]
C_3	1.19 (-7)	2.20 (-15)	8.76 (-19)	2.90 (-17)	8.22 (-16)	1.41 (-15)	
C_2H	5.46 (-5)	6.65 (-10)	5.55 (-13)	1.08 (-11)	1.45 (-11)	6.57 (-13)	
C_2H_2	1.56 (-4)	2.82 (-4)	2.81 (-4)	2.80 (-4)	2.69 (-4)	2.58 (-4)	8.0 (-5)[1]
C_3H_2	8.11 (-11)	1.87 (-12)	5.28 (-12)	1.37 (-11)	1.13 (-11)	1.09 (-11)	
CH	1.89 (-8)	3.87 (-13)	3.23 (-20)	2.10 (-19)	2.50 (-21)	3.69 (-22)	
CH_2	2.21 (-8)	5.16 (-11)	2.24 (-16)	3.65 (-18)	2.28 (-21)	1.50 (-22)	
CH_3	4.79 (-8)	4.08 (-8)	1.68 (-11)	1.22 (-15)	1.29 (-18)	4.84 (-19)	
CH_4	6.92 (-9)	9.22 (-7)	2.74 (-8)	6.58 (-15)	5.69 (-19)	1.02 (-19)	Low[1]
SiN	7.24 (-10)	2.64 (-9)	3.08 (-9)	4.51 (-10)	1.86 (-10)	3.84 (-10)	
NH	2.06 (-11)	2.28 (-14)	1.12 (-18)	3.96 (-20)	1.23 (-22)	2.92 (-25)	
NH_2	7.53 (-12)	8.31 (-13)	1.17 (-15)	5.41 (-20)	4.78 (-24)	1.10 (-27)	
NH_3	9.02 (-12)	3.83 (-11)	9.56 (-12)	3.07 (-18)	3.26 (-23)	1.59 (-26)	Low[1]
SiH	1.96 (-7)	1.67 (-6)	2.93 (-6)	6.57 (-10)	1.13 (-11)	1.07 (-12)	
SiH_2	1.07 (-10)	1.11 (-7)	7.12 (-7)	5.51 (-10)	2.42 (-11)	8.00 (-11)	
SiH_3	4.60 (-12)	2.52 (-9)	3.28 (-8)	1.29 (-10)	2.54 (-11)	1.02 (-10)	
SiH_4	1.35 (-16)	2.28 (-11)	3.75 (-9)	1.84 (-10)	8.91 (-11)	2.08 (-10)	Low[1]
CN	5.23 (-7)	2.36 (-11)	5.26 (-14)	2.83 (-12)	7.49 (-12)	8.37 (-13)	
HCN	5.11 (-5)	3.25 (-6)	2.82 (-6)	3.19 (-6)	3.14 (-6)	3.01 (-6)	4.0 (-5)[5]
N_2	6.30 (-5)	9.63 (-5)	9.66 (-5)	9.61 (-5)	9.26 (-5)	8.88 (-5)	
HNSi	1.67 (-10)	1.67 (-8)	1.84 (-9)	3.46 (-10)	1.23 (-10)	1.17 (-10)	
HCS	4.60 (-10)	2.56 (-13)	2.73 (-14)	4.26 (-15)	1.37 (-14)	9.57 (-14)	
HCO	6.53 (-12)	1.60 (-11)	2.82 (-13)	8.54 (-12)	7.90 (-12)	1.20 (-11)	
SiO	1.86 (-8)	4.90 (-6)	7.26 (-7)	4.27 (-7)	2.73 (-7)	2.64 (-7)	8.0 (-7)[1]
CO	9.79 (-4)	1.07 (-3)	1.08 (-3)	1.08 (-3)	1.04 (-3)	9.95 (-4)	8.0 (-4)[4]
OH	5.35 (-13)	4.56 (-15)	1.81 (-23)	0.			
H_2O	1.66 (-11)	1.16 (-10)	2.03 (-16)	2.85 (-19)	1.52 (-22)	1.61 (-22)	

"very fast chemistry" region in which the inputs from the immediate postshock region are quickly changed. Therefore the final abundances listed in Table 4 depend only on the parameters characterising the gas excursion associated with a particular shock strength. Secondly, molecular abundances injected in the intermediate envelope are the results of an active shock-induced chemistry in the very inner envelope because rapid freeze-out of the chemistry occurs for damped and weak shocks at a few stellar radii.

3.2. Silicon and sulphur species

SiS, SiO and CS are known as "parent" molecules and their IR ro-vibrational bands were observed in IRC+10216 close to the star (Keady & Ridgway 1993, Boyle et al. 1994). Millimetre emission maps show clearly that SiS and CS are centered on the star (Lucas et al. 1995). Abundances derived from observations were often compared mistakenly to TE values calculated for flow conditions that correspond to regions at several stellar radii from the photosphere (Lafont et al. 1982). However, TE holds only in the photosphere and within the shock formation radius (Cherchneff & Tielens 1992). Inspection of Table 4 shows that SiO has a very low abundance at the shock formation radius, a value ~ 40 times smaller than that derived by Keady & Ridgway (1993) at ~ 10 R$_\star$, implying that the molecule must form efficiently in the inner envelope. For SiS, the TE abundance is consistent with the observations but SiS is in fact processed in the inner wind.

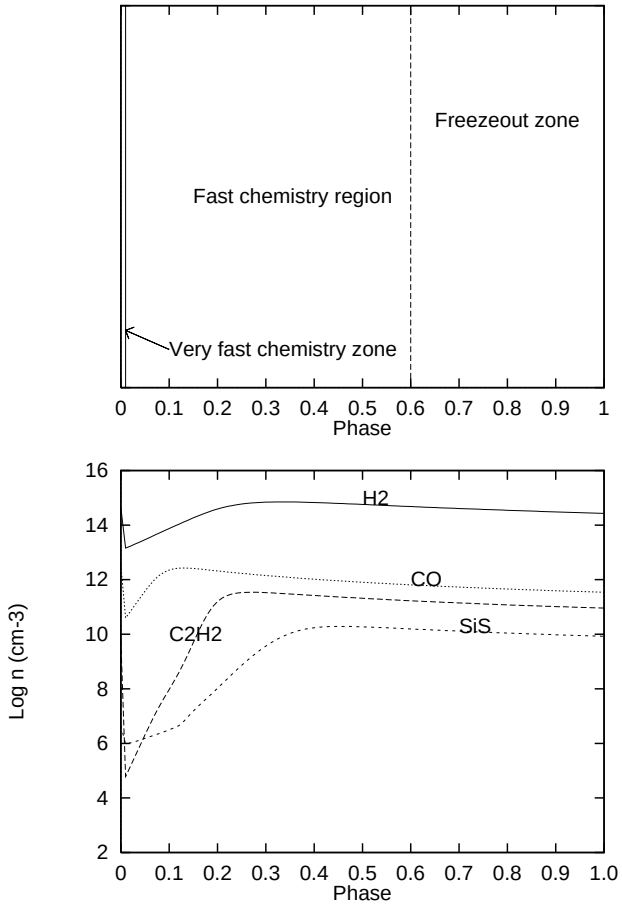

Fig. 4. The excursion can be divided into three regions depending on the relative values of the chemical and dynamical timescales. This is illustrated here at 20kms^{-1}

Our results show that SiO is produced in the excursion induced by the fastest shocks from the reaction

$$\mathrm{Si + OH \longrightarrow SiO + H} \quad (6)$$

OH is formed in the immediate postshock region and at the beginning of the excursion associated with large shock strengths (see Sect. 3.4). SiO destruction processes are

$$\mathrm{SiO + H \longrightarrow Si + OH} \quad (7)$$

$$\mathrm{SiO + H \longrightarrow SiH + O} \quad (8)$$

At lower shock strengths destruction is by Reaction 7, together with an addition destruction process

$$\mathrm{SiO + M \longrightarrow Si + O + M} \quad (9)$$

for which the reaction rate has been estimated. SiO is therefore a product of the chemistry due to the propagation of fast shocks in the inner envelope and its formation is linked to the temporary formation of oxygen-bearing molecules in the immediate postshock region and at the beginning of the gas excursion.

At slower shock speeds, freeze-out dominates the excursion and the abundance of SiO starts to level off for $\Delta v \leq 11.7$ kms^{-1}. Our theoretical concentration at 5 R$_\star$ is in good agreement with the observational value, a result which supports our estimated rates for the gas collider reactions.

The formation process for silicon sulphide, SiS, involves the formation of HS in the gas excursions and the following reactions:

$$\mathrm{S + H_2 \longrightarrow HS + H} \quad (10)$$

$$\mathrm{S + C_2H_2 \longrightarrow C_2H + HS} \quad (11)$$

$$\mathrm{HS + Si \longrightarrow SiS + H} \quad (12)$$

These reactions have activation energy barriers and therefore occur mainly in the hot "fast chemistry" zone of excursions induced by fast shocks (see Fig. 1). For excursions induced by slower shock strengths, SiS is formed by the termolecular reaction

$$\mathrm{Si + S + M \longrightarrow SiS + M} \quad (13)$$

Reactions (11), (12) and (13) have estimated rates but the good agreement of our SiS theoretical abundance with the observational value implies that our guesses are reasonable. Obviously, the agreement can be improved by fine-tuning the reaction rates involved in the formation processes.

The P-branch transitions of the ro-vibrational fundamental band of carbon sulphide, CS, have been observed by Keady & Ridgway (1993). They derive an abundance at 5 R$_\star$ of 4×10^{-6} from modelling the ro-vibrational lines with a decrease in the abundance at $r > 14$ R$_\star$ to account for the low J lines. The TE abundance at r_s is 3 times larger than the observational value and our model shows again how the non-equilibrium, shocked inner layers govern the chemistry of chemical species. For the fastest shock strength, CS is destroyed in the excursion by the reaction

$$\mathrm{SiC + CS \longrightarrow SiC_2 + S} \quad (14)$$

which is efficient as SiC is still present at r_s (see Table 4). As a result, the CS abundances decreases by 7 orders of magnitude compared to its TE value. For smaller shock strengths, CS gradually reforms from the following processes

$$\mathrm{C_3 + S \longrightarrow CS + C} \quad (15)$$

and

$$\mathrm{CN + S \longrightarrow CS + N} \quad (16)$$

Our theoretical abundance of CS at 5 R$_\star$ is lower by a factor ~ 6 than the observed value but we consider the result satisfying in view of the uncertainties entering both theoretical and observational models. As for SiO and SiS, the important point is that molecular abundances are highly altered and processed in the shocked region of the inner envelope.

There exists no IR observation of SiC_2 close to the star but mm observations of the outer envelope show that the molecule is present at $r < 100R_\star$ with an abundance smaller than 5×10^{-8} (Gensheimer et al. 1995). SiC_2 has a large TE abundance in the photosphere and at r_s which does not agree with the above upper limit. However, its abundance is reset by the non-equilibrium chemistry occurring in the "very fast chemistry" zone of the excursions associated with fast shocks. The main formation and destruction processes are

$$Si + C_2H \longrightarrow SiC_2 + H \quad (17)$$

and its reverse process which becomes dominant at slower shock strengths. The SiC_2 abundance at the end of the inner envelope is much less than its TE value and agrees with the value derived by Gensheimer et al. (1995). Again, this result supports our estimated rate for Reaction (17) using rates involving covalent species.

3.3. CH_4, NH_3 and SiH_4

Methane (CH_4), ammonia (NH_3) and silane (SiH_4) are believed to form in the intermediate envelope from gas-grain interactions. Indeed, their TE abundances in the photosphere are low and the ro-vibrational lines observed by Keady & Ridgway (1993) are reproduced using non-monotonic, truncated molecular distributions for these species. Our results confirm that the molecules are definitely absent from the inner wind (as illustrated in Table 4), in particular ammonia and methane, which are present in the photosphere, but are destroyed in the inner wind via collisions with H. As for SiH_4, the molecule is formed in the shock-induced oscillations but our final theoretical abundances remains low.

3.4. Oxygen-bearing molecules

Several oxygen-bearing molecules are formed in the postshock region of the fastest shocks. In the immediate postshock region and the "very fast chemistry" zone of the excursion, CO is destroyed by collision with atomic H to release free O atoms. At the start of the excursion, atomic oxygen reacts with atomic S to form SO. OH then forms from

$$SO + H \longrightarrow OH + S \quad (18)$$

and from

$$O + H_2 \longrightarrow OH + H \quad (19)$$

Water, H_2O, subsequently forms from reaction

$$OH + H_2 \longrightarrow H_2O + H \quad (20)$$

In the "fast chemistry" region, the reverse reactions of both processes become dominant and H_2O and OH are gradually destroyed at large phase. As previously mentioned, the formation of oxygen-bearing species in the postshock gas of the fast shocks triggers the formation of SiO. These oxygen-rich species may also affect the dust nucleation processes as oxygen is known to inhibit the growth of large carbon chains and polycylic aromatic hydrocarbons (Frenklach & Feigelson 1996). Our results show that, apart from CO, SiO and to a less extent HCO, the inner wind of IRC+10216 is depleted of oxygen-rich bearing chemical species.

3.5. Discussion

The present study shows that the inner envelope of IRC+10216 is a region of active chemistry. Indeed, several molecules which were believed to originate from the stellar photosphere under TE conditions are formed in this highly non-equilibrium region (e.g. SiO). Other molecules which are overabundant at TE in the photosphere are destroyed in the inner wind and their abundances are then governed by the non-equilibrium chemistry of the inner envelope (e.g. CS and SiC_2). The good agreement between theoretical and observational abundances validates our dynamical and chemical models of IRC+10216 inner envelope, although a full description of the chemical processes is an impossible task as many reaction rates have not yet been measured in the laboratory or predicted by theory. As for the dynamical model, it seems that our simple analytical description is satisfactory in reproducing the gas parameter variations.

An important point to mention is that the inner envelope corresponds to the wind acceleration zone where dust grains are expected to form. The dominant formation processes for amorphous carbon dust nucleation initiate with the conversion of acetylene C_2H_2 into larger hydrocarbons (Frenklach & Feigelson 1996). This conversion can occur via isomerisation of acetylene as in soot formation processes in acetylenic flames or via direct infrared pyrolysis (Herlin et al. 1997). We did not consider the chemistry of dust nucleation in our model because only a small fraction of acetylene is converted into large aromatic molecules. The nucleation and condensation of dust grains will change the physical conditions in the gas as dust will quickly accelerate the wind and generate a high mass loss. However, the stationary layers we have described in this study will still be present as the dust condensation occurs only for a narrow range of gas parameters which are found at radii larger than $3 - 4$ $R_\star$ (Cherchneff 1997). Therefore the layers close to the stellar photosphere represent the locus of active molecule and dust formation.

Another condensate of interest in the inner envelope is silicon carbide SiC. Infrared pyrolysis of silane and acetylene produces SiC condensates very efficiently and it was proposed that the formation of atomic Si and SiC_2 triggers the nucleation of SiC grains via the reaction

$$Si + SiC_2 \longrightarrow 2\ SiC \quad (21)$$

and the subsequent coalescence of SiC molecules into solid particles (Lihrmann & Cauchetier 1994). This reaction has an endothermicity of $\sim$ 395 kJ mole^{-1} at 1000 K and is not included in our chemical scheme listed in Table 5. Inspection of Table 4 shows that SiC gaseous is absent from the inner envelope as it is quickly destroyed in the shock-induced excursions.

However, the abundance of atomic Si is quite high and constant in the inner envelope and SiC_2 is also present in the flow. Assuming that the SiC_2 abundance is used in forming SiC particles with average radius 100Å following Reaction (21), the total abundance of SiC grains relative to the total gas concentration would be $\sim 1 \times 10^{-14}$. Bagnulo (1996) has fitted the spectral energy distribution (SED) of IRC+10216 using an amorphous carbon-to-gas and a SiC-to-gas ratio of 5×10^{-3} and 3×10^{-4}, respectively. The SiC component corresponds to an abundance of $\sim 2 \times 10^{-11}$ assuming 100Å radius SiC grains and the total dust-to-gas ratio derived by Knapp & Morris (1985). This value is 3 orders of magnitude larger than that derived from our SiC_2 abundance. If the upper limit derived by Gensheimer et al. (1995) for the SiC_2 inner abundance is used, the SiC solid abundance derived from fitting SEDs is still larger by a factor ~ 50. This simple analysis implies that other mechanisms to form SiC grains must occur in the inner wind of IRC+10216.

Future studies will investigate the coupling of the silicon-sulphur chemistry and the dust nucleation-condensation processes. We will also investigate the gas-solid phase chemistry occuring in the intermediate envelope.

Acknowledgements. The authors wish to thank the referee, J. J. Benayoun, for useful comments on how to improve the manuscript, and P. Sarre and M. Costes for helpful discussions.

References

Allendorf M. D., Mellius C. F., 1992, J. Phys. Chem. 96, 428
Bagnulo S., 1996, PhD Thesis, The Queen's University of Belfast, N. Ireland
Baulch D. L., Cobos C. J., Cox R. A., Esser C., Franck P., Just Th., Kerr J. A., Pilling M. J., Troe J., Walker R. W., Warnatz J., 1992, J. Phys. Chem. Ref. Data 21, 411
Benson S., 1976, Thermodynamical Kinetics. Wiley, New York
Bertschinger E., Chevalier R. A., 1985, ApJ 299, 167
Bowen G. H., 1988, ApJ 329, 299
Boyle R. J., Keady J. J., Jennings D. E., Hirsch K. J., Wiedermann G. R., 1994, ApJ 420, 863
Chase M. W., Davies C. A., Downey J. R., Frurip D. J., McDonald R. A., Syverud A. N., 1985, J. Phys. Chem. Ref. Data 14, Suppl. 1, 1
Cherchneff, I., 1997, in: E.F. van Dishoeck (ed.) Proc. IAU Symp. 178, Molecules in Astrophysics: Probes and Processes. Kluwer, Dordrecht, p. 469
Cherchneff I., Glassgold A., 1993, ApJ 419, L41
Cherchneff I., Glassgold A, Mamon G., 1993, ApJ 410, 188
Cherchneff I., Tielens, A. G. G. M., 1994, in: R. Clegg, I. Stevens, & W.P.S. Meikle (eds.) Circumstellar Media in the Late Stages of Stellar Evolution. Cambridge University Press, Cambridge, p 232.
Cherchneff I., Tielens, A. G. G. M., 1997, in preparation
Cherchneff I., Barker J. R., Tielens A. G. G. M., 1991, ApJ 377, 541
Cherchneff I., Barker J. R., Tielens A. G. G. M., 1992, ApJ 401, 269
Fitzgerald et al., 1986, J. Chem. Phys. 85, 1701
Frenklach M., Feigelson E., 1996, in: Y. Pedleton (ed.) Proc. ASP Symp., From Stardust to Planetesimals. in press
Fox M. W., Wood P. R., 1985, ApJ 297, 455
Gensheimer P. D., Likkel L., Snyder L. E., 1995, ApJ 439, 455
Herlin N., Bohn I., Reynaud C., Cauchetier M., 1997, A&A, submitted
Hinkle K. H., Hall D. N., Ridgway S. T., 1982, ApJ 252, 697
Keady J. J., Hinkle K. H., 1988, ApJ 331, 539
Keady J. J., Ridgway S. T., 1993, ApJ 406, 199
Knapp G. R., Morris M., 1985, ApJ 292, 640
Lafont S., Lucas R., Omont A., 1982, A&A 106, 201
Lihrmann J. M., Cauchetier M., 1994, J. European Ceramic Soc. 13, 41
Lucas R., Guélin M., Kahane C., Audinos P., Cernicharo J., 1995, Ap & SS 224, 293
MacKay D. D. S., 1996, MNRAS 274, 694
Mallard W. G., Westley, F., Herron J. T., Hampson R. F., Frizzell D. H., 1994, NIST Chemical Kinetics Database: Version 6.0, National Institute of Standards and Technology, Gaithersburg (MD)
Mick H. R., Roth P., Smirnov V. N., Zaslonko I. S., 1994, Kinetics & Catalysts 35, 485
Millar T. J., Farquhar P. R. A., Willacy K., 1997 A&AS 121, 139
Millar T. J., Herbst E., 1994, A&A 288, 561
Olofsson H., 1997, in: E.F. van Dishoeck (ed.) Proc. IAU Symp. 178, Molecules in Astrophysics: Probes and Processes. Kluwer, Dordrecht, p. 457
Wiedemann G. R., Hinkle K. H., Keady J. J., Deming P., Jennings D. E. 1991, ApJ 382, 321
Willson L. A., Bowen G. H., 1984, in: R. Stalio & J.B. Zirker (eds.) Relation between Chromospheric Coronal Heating and Mass Loss in stars. Triestre Workshop Series, Triestre, p. 127
Zuckerman B., Terzian Y., Silverglate P., 1980, ApJ 241, 1014

This article was processed by the author using Springer-Verlag LaTeX A&A style file *L-AA* version 3.